JOURNAL OF PETROLEUM AND GEOTHERMAL TECHNOLOGY
ISSN: 2723-0988, e-ISSN: 2723-1496
Vol.4 No. 2 2023

Improving Well Productivity through the Combination of Deep Penetrating Perforation and High Energy Gas Fracturing Techniques

Fanata Yudha Nugraha [1*)], Brian Tony [1)], Angelica Catharine Zefanya[1)], Nur Ilham Tarsila[1)], Damar Nandiwardhana[1)]
[1)] Petroleum Engineering, Universitas Pembangunan Nasional Veteran Yogyakarta
*Corresponding email: fanata.yudha@upnyk.ac.id

ABSTRACT

Perforation operations often result in formation damage and compacted zones, which can increase skin effects and decrease well productivity. To address these issues, a combination of deep penetrating perforation and high-energy gas fracturing techniques can potentially solve these problems. This study utilized commercial software to simulate perforation and fracture geometry and evaluated productivity using parameters such as skin effect, productivity index, and inflow performance relationships. The methodology used in this research can be broken down into three main steps: First, simulation modeling of deep penetrating perforation and high-energy gas fracturing is performed to determine the resulting perforation and fracture geometry. The high-energy gas fracturing is modeled using a hydraulic fracturing approach. Second, the productivity results are evaluated against the obtained geometry using parameters such as skin, productivity index, and inflow performance relationship. Finally, the productivity results obtained using the combination of deep penetrating perforation and high-energy gas fracturing are compared with the productivity results of conventional perforation techniques. Results showed that the combination technique increased productivity by 3.34 times compared to conventional perforation and 2.45 times compared to standalone deep penetrating perforation. This suggests that the combination technique effectively improves well productivity by reducing the skin effect and increasing the productivity index and flow rate. Overall, the study provides promising evidence for the effectiveness of the combination technique in improving well productivity.

Keywords: deep penetrating perforation; geometry; high-energy gas fracturing; inflow performance relationship (IPR); productivity index (PI); skin effect

I. INTRODUCTION

Perforation is a critical process in oil and gas well completion that involves creating openings in the well casing and surrounding rock formations to allow for the flow of hydrocarbons. Jet gun perforators have been widely used for perforation operations since 1946, replacing the previous bullet perforators (Schechter, 1992). However, the jet gun perforator has a major issue: it creates a damaged zone around the perforation holes, commonly known as a compacted or crushed zone. This compacted zone can form a skin around the perforation holes, ultimately reducing the efficiency of the production flow rate from the reservoir into the wellbore. Additionally, another issue commonly encountered during perforation operations is near wellbore formation damage, which is a formation zone around the wellbore that has reduced porosity and permeability as a result of fluid invasion, drilling mud, and completion cement. This zone can impede the oil-gas production flow rate during the production process. Previous studies have extensively discussed these issues (Klotz et al., 1974; El-Bermawy, 2001; Krueger, 1988; Lea et al., 1991; Halleck, 1997). With the development of technology, a new method has been discovered that can address the issues associated with conventional perforation techniques. This method involves combining deep penetrating perforation and high-energy gas fracturing techniques.

This study aims to prove the effectiveness of the combination of deep penetrating perforation and high-energy gas fracturing techniques on well productivity through simulation modeling. In this study, the authors also performed modeling of the geometry and evaluated its impact on production parameters, which has not been previously investigated.

1.1 Deep Penetrating Perforation

Deep penetrating perforation is a method utilized in oil and gas well operations to generate perforation holes that deeply penetrate the reservoir formation. This technique aims to improve well productivity by providing improved access to the hydrocarbon-rich zones. Specialized tools and charges are utilized in deep penetrating perforation to create perforations that penetrate deeper into the formation, consequently enhancing the flow of oil or gas from the reservoir into the wellbore. The depth of penetration can vary depending on the particular well conditions, properties of the formation, and the objectives of the operation. Deep penetrating (DP) perforation is a perforation mechanism primarily used in hard

formations. Typically, deep penetrating (DP) perforation creates perforation holes with diameters ranging from 0.2 to 0.5 inches and penetration depths reaching several inches (Halliburton, 2017). According to API RP 19B (2001), the penetration depth of deep penetrating perforation can reach 60 inches or more.

1.2 High-energy Gas Fracturing

High-energy gas fracturing is a technique used to increase the productivity of oil and gas wells by creating fractures in the formation. This technique differs from hydraulic fracturing in that it utilizes gunpowder or propellant combustion within the wellbore to generate high-pressure gas that is then directed into the perforation hole to form fractures. The pressure resulting from the combustion of propellant typically lasts for a very short time, usually only between 10 and 100 milliseconds (El-Bermawy, 2001). Gunpowder or propellant has a slower combustion rate compared to high-explosive-shaped charges. Shaped charges are detonated under rapid, high pressure that lasts for microseconds. In contrast, propellant is designed to burn at a lower pressure and slower speed, taking milliseconds to burn. Hydraulic fracturing, on the other hand, is characterized by a slower pressure rate than both of these methods and usually takes several seconds to complete (Albert et al, 2018).

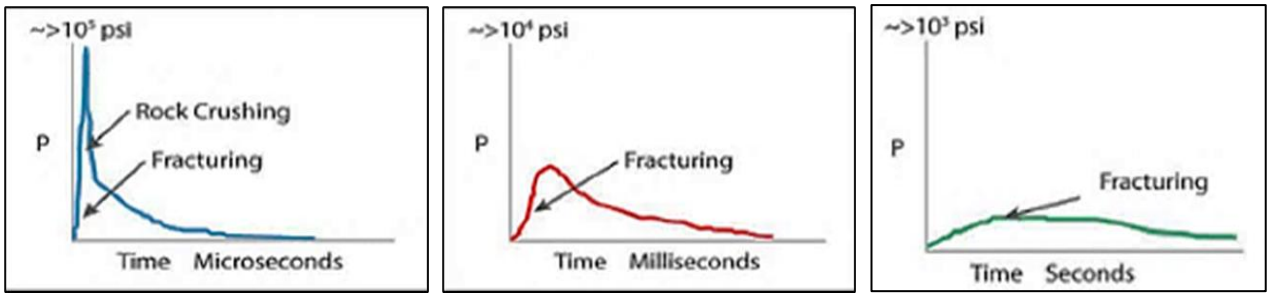

(a) (b) (c)

Figure 1. Pressure-Time Plot (a) High Explosives Shaped Charge, (b) Propellant, (c) Hydraulic Fracturing
Source: Albert et al, 2018

II. METHODS

The methodology used in this research can be broken down into three main steps: First, simulation modeling of deep penetrating perforation and high-energy gas fracturing is performed to determine the resulting perforation and fracture geometry. The high-energy gas fracturing is modeled using a hydraulic fracturing approach. Second, the productivity results are evaluated against the obtained geometry using parameters such as skin, productivity index, and inflow performance relationship. Finally, the productivity results obtained using the combination of deep penetrating perforation and high-energy gas fracturing are compared with the productivity results of conventional perforation techniques.

2.1 Modeling Process Using Software

The process of creating the necessary models for this study involves two parts: modeling of perforation and modeling of high-energy gas fracturing. The details are as follows:

a) Perforation Modeling

The modeling of perforation was carried out using *Pipesim 2017* software, which aimed to determine the geometry of both conventional and deep penetrating perforation operations, including the density, length, and diameter of the perforation, as well as the analysis of the impact of both perforation techniques on production, specifically skin damage. The data required to create this model includes tubular data, completion data, reservoir data, formation data, and perforation interval data. Additionally, information on the thickness and permeability of the formation-damaged zone, as well as the thickness and permeability of the compacted zone, is also required. In creating the perforation model, modeling was carried out with different perforation system cases in each productive layer, with the details shown in **Table 1**.

The perforation system specification describes the types of guns and explosive charges used in each perforation system. Charge weight explains the mass or weight of the explosive charge for each individual perforating charge in each perforating gun. Gun OD refers to the outer diameter of the perforating gun. API penetration describes the length of penetration of the resulting perforation hole based on the reference of the API RP test edition. API entrance hole explains the diameter of the entry hole of the resulting perforation hole based on the reference of the API RP test edition. API test edition specifies the edition of the American Petroleum Institute standard used for testing the gun system, and it is from this API edition that the length of penetration and diameter of the perforation hole are determined. The penetration model is the type of target used in perforation tests based on the API reference used.

Table 1. Perforation system case

Case	Perforation system	Charge weight	Gun OD	Phase Angle	Perforation Density	API Penetration	API entrance hole	API test edition	Penetration model
		gram	in	degree	Shots/ft	in	in		
1	*5" HSD, 43C UltraPack RDX*	24,00	5,00	72	5	9,79	0,61	RP43 5th edition	Concrete based
2	*4,72" PURE, PowerJet Omega 3506, HMX*	27,00	4,72	135/45	12	44,20	0,44	RP19B 1st edition	Rock based
3	*4,72" PURE, PowerJet Nova3406, HMX*	22,50	4,72	135/45	12	42,90	0,40	RP19B 1st edition	Rock based
4	*5" HSD, PowerJet Omega 4505, HMX*	38,80	5,00	72	5	65,20	0,45	RP19B 1st edition	Rock based
5	*5" HSD, PowerJet Nova 4505, HMX*	45,00	5,00	72	5	57,40	0,34	RP19B 1st edition	Rock based

b) High-energy Gas Fracturing Modeling

High-energy gas fracturing modeling is performed using *Fraccade 7.0* software. The required data includes perforation geometry data such as the density, length, and diameter of the perforation from the previous perforation modeling step. Additionally, input data customization is necessary for fracturing fluid properties and proppant properties.

The objective of using *Fraccade 7.0* for simulating high-energy gas fracturing is to predict fracture geometry, including the length, height, and width of the fracture, as well as dimensionless fracture conductivity (C_{FD}), which will be used to evaluate productivity results. The detailed data used for high-energy gas fracturing design is shown in **Table 2.**

Table 2. Deep Penetrating Perforation Data

Zone	Top TVD (ft)	Thick zone (ft)	SPF	Total Shots	Tunnel Diameter (in)	Tunnel Length, (in)	Method
Shale 1	3600,0	56,5	0	0	0	0	Underbalanced
Shale 2	3656,5	98,0	0	0	0	0	Underbalanced
Shale 3	3754,5	18,5	0	0	0	0	Underbalanced
Sandstone 1	3773,0	13,5	4,67	63	0,89	27,25	Underbalanced
Shale 4	3786,5	2,5	0	0	0	0	Underbalanced
Sandstone 2	3789,0	4,5	4,0	18	0,89	27,24	Underbalanced
Shale 5	3793,5	22,5	0	0	0	0	Underbalanced
Sandstone 3	3816,0	3,5	3,71	13	0,89	27.22	Underbalanced
Shale 6	3819,5	12,5	0	0	0	0	Underbalanced
Sandstone 4	3832,0	7,5	4,53	34	0,89	27,21	Underbalanced
Shale 7	3839,5	43,5	0	0	0	0	Underbalanced
Sandstone 5	3883,0	3,5	0	0	0	0	Underbalanced
Shale 8	3886,5	33,5	0	0	0	0	Underbalanced
Sandstone 6	3920,0	2,5	0	0	0	0	Underbalanced
Shale 9	3922,5	4,0	0	0	0	0	Underbalanced

Fracturing Fluid and Proppant Customization

The first adjustment or customization is related to the fracturing fluid used in high-energy gas fracturing modeling. The author assumes that under actual conditions, the combustion of propellant in high-energy gas fracturing will result in the formation of CO_2 gas in the liquid CO_2 phase. This is due to the high pressure and temperature generated during propellant combustion, which surpasses the critical point of CO_2 gas, causing it to transition into the liquid phase ((Liu, et al.,2014). Therefore, customization is carried out for the type of fluid and viscosity, namely Base Fluid of *ClearFrac 25* (liquid CO_2) and viscosity of 0,16 cP.

The second customization is performed on the proppant. The purpose of customizing the proppant is to approximate the actual conditions in high-energy gas fracturing, where the proppant is not used in the fracturing operation (Zazovsky,

2004). In this study, the use of proppant in high-energy gas fracturing modeling is not intended as a fracture propping agent, as in conventional fracturing modeling, but rather as a simulation of the presence of fine rock grains or particles formed after the rock fracturing process. Therefore, customization of the proppant is necessary to resemble the formation's rock grains, which in this study are sandstones, as indicated in **Table 3**.

Table 3. Proppant Data

Type	Nature sand
Mesh size	80/100
Diameter, in (Robert, 1982)	0,005
Specific gravity (Feng, et al., (2015)	2,65
Bulk density, lb/gal (Feng, et al., (2015)	22,115
Permeability, mD	19736

Pump Scheduling

High-energy gas fracturing modeling in this research is using approachment of hydraulic fracturing, so that is needed pump scheduling like the conventional hydraulic fracturing. To be considered that the actual high-energy gas fracturing does not require pump scheduling for injecting the fluid frac and proppant. The actual high-energy gas fracturing uses the combustion of gun powder or propellant in the wellbore that will be generating high pressure CO_2 gas to form fracture in the formation. This pump scheduling is an approach to simulate the effect of customized high pressure CO_2 gas in forming fracture, as well as knowing the effect of customized proppants on the effective conductivity of the fractures that have been formed. Pump scheduling can be seen in **Table 4** below.

Table 4. Pump Scheduling

Step Name	Pump Rate, (bbl./min)	Fluid Name	Fluid Volume, (Gal)	Proppant	Proppant Conc. (PPA)	Proppant Mass, (lb.)	Slurry Vol, (bbl.)
Pad	2	Customized liquid CO_2	1500	Customized sand	0	0	35,7
2,0 PPA	2		75		2	150	1,9
4,0 PPA	2		75		4	300	2,1
6,0 PPA	2		75		6	450	2,3
8,0 PPA	2		75		8	600	2,4
10,0 PPA	2		75		10	750	2,6
12,0 PPA	2		75		12	900	2,8
14,0 PPA	2		75		14	1050	2,9
16,0 PPA	2		75		16	1200	3,1
18,0 PPA	2		75		18	1350	3,2
20,0 PPA	2		75		20	1500	3,4
22,0 PPA	2		75		22	1650	3,6
24,0 PPA	2		75		24	1800	3,7
26,0 PPA	2		75		26	1950	3,9
28,0 PPA	2		75		28	2100	4,0
Flush	2	Brine	6238	-	0	0	148,5

2.2 Productivity Evaluations

The evaluation of productivity results is conducted in three cases: conventional perforation, deep penetrating perforation, and a combination of deep penetrating perforation and high-energy gas fracturing. The parameters used in evaluating productivity are skin effect, productivity index (PI), and inflow performance relationship (IPR).

a) Skin Effect Evaluation

In this study, the focus is on mechanical skin, which is the total sum of previously obtained skin. From the skin value, the authors can evaluate the impact of perforation geometry, both conventional and deep penetrating perforation, on the resulting skin damage which ultimately affects well productivity.

Skin value from both perforation, conventional and deep penetrating operation, can be known directly from *Pipesim 2017* after conducting perforation modeling. Determining the skin value in high-energy gas fracturing modeling is using Prats methods for fracturing evaluation approach. Prats converts the function of fracture length (*xf*) and dimensionless fracture conductivity (C_{FD}) as the effective well radius (r_w') for pseudo radial flow. This effective well radius depicts the response of well radius (r_w) which is widened due to the fracture formed (Smith, et al., 2000). Prats' method for evaluating fractures uses some assumptions which are, steady-state flow conditions, cylindrical encouragement, incompressible fluids, and the fracture height is equal to formation (pay zone) height (Smith, et al., 2000). Prats' method can be seen as **Figure 2** below.

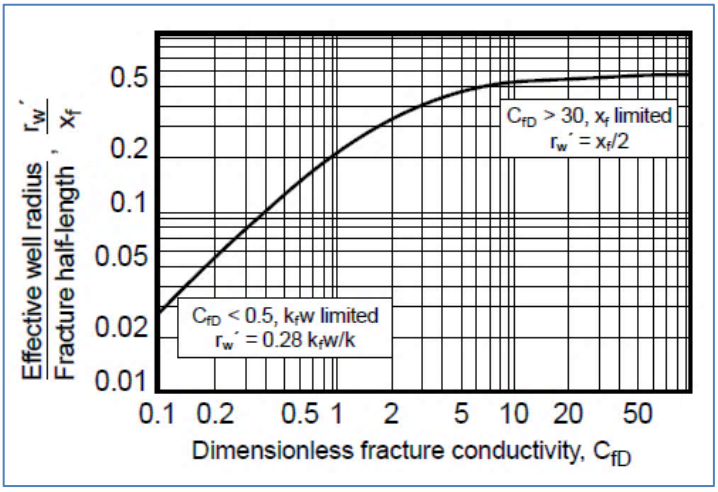

Figure 2. Prats' Correlation Graph
Source: Smith, et al., 2000

The fracture length (*xf*) and dimensionless fracture conductivity (C_{FD}) obtained from high-energy gas fracturing modeling can be used for determining the effective well radius (r_w') using the graph above. Next, the effective well radius (r_w') is used for predicting skin value after fracturing with **Equation 1** below.

$$Sf = - ln\ (r_w'/r_w) \qquad (1)$$

b) Productivity Index (PI) Evaluation

The productivity index (PI) is a measure that describes the potential of a reservoir to flow or produce fluid to the wellbore. PI evaluation was carried out on the results of both perforation and high-energy gas fracturing modeling. This research uses assumptions of radial flow and steady-state flow regime for estimating the productivity index, with the Darcy equation (Guo, et all., 2007) as seen in **Equation 2** below.

$$PI = \frac{k\,h}{141{,}2\,\mu_o\,B_o\left(ln\frac{r_e}{r_w} + S\right)} \qquad (2)$$

c) Inflow Performance Relationship (IPR) Evaluation

In this research, inflow performance relationship (IPR) is used to evaluate reservoir deliverability for both, perforation and high-energy gas fracturing modeling. IPR evaluation was carried out manually using Vogel method. Vogel's IPR assumes that reservoir pressure is below the bubble point pressure of hydrocarbon fluids, so there will be two-phase fluid in the reservoir (Guo, et all., 2007). Vogel's IPR can be constructed by **Equation 3** and **Equation 4**, as seen below.

$$q_{max} = \frac{J\bar{p}}{1{,}8} \qquad (3)$$

$$q = q_{max}\left[1 - 0{,}2\left(\frac{p_{wf}}{\bar{p}}\right) - 0{,}8\left(\frac{p_{wf}}{\bar{p}}\right)^2\right] \qquad (4)$$

III. RESULTS AND DISCUSSION

The data produced in this study focuses on the modeled perforations' geometry, evaluation of skin values, and productivity results, as outlined below:

3.1 Perforation Geometry Modeling Results

The perforation modeling results of each perforation system for all formations are presented in **Table 5** below. To enhance understanding of the perforation geometry based on the modeling results, this study includes schematic representations illustrating the perforation geometry for each perforation system case in sandstone layer 1 (**Figure 3**). The analysis reveals consistent values for the length and diameter of the perforation holes across all productive layers in the cases. This consistency arises from the limited availability of reservoir data obtained for each productive layer.

Importantly, it is observed that the length of the perforation holes generated using different software is comparatively shorter or reduced compared to the holes modeled by the API. This difference can be attributed to various influencing factors, including the gun carrier, casing, cement, and formation that the perforation must penetrate. These factors significantly decrease the energy required for perforation hole formation, resulting in variations or reductions in hole length compared to the API modeling results. Additionally, the specifications of the casing (grade and density) and the density of the cement used also impact the length of the resulting perforation holes. Higher casing specifications and cement density lead to a substantial reduction in the energy required for perforation formation, resulting in shorter hole lengths.

Table 5. Perforation Geometry Modeling Results

Case	Perforation System	Total penetration Average, (in)				Casing entrance hole diameter average, (in)				Formation penetration Average, (in)				Formation diameter average, (in)			
		Sandstone				Sandstone				Sandstone				Sandstone			
		1	2	3	4	1	2	3	4	1	2	3	4	1	2	3	4
1	*5" HSD 43C UltraPack RDX*	8,69	8,69	8,68	8,67	0,62	0,62	0,62	0,62	7,87	7,87	7,86	7,85	2,08	2,08	2,08	2,08
2	*4,72" PURE PowerJet Omega 3506 HMX*	21,74	21,73	21,71	21,69	0,37	0,37	0,37	0,37	20,92	20,91	20,89	20,87	0,88	0,88	0.88	0,88
3	*4,72" PURE PowerJet Nova3406 HMX*	24,11	24,10	24,07	24,05	0,40	0,40	0,40	0,40	23,29	23,28	23,25	23,23	0,96	0,96	0,96	0,96
4	*5" HSD, PowerJet Omega 4505 HMX*	26,13	26,12	26,10	26.08	0,50	0,50	0,50	0,50	25,32	25,31	25,28	25,26	1,18	1,18	1,18	1,18
5	*5" HSD PowerJet Nova 4505 HMX*	28,07	28,06	28,04	28,02	0,37	0,37	0,37	0,37	27,25	27,24	27,22	27,21	0,89	0,89	0,89	0,89

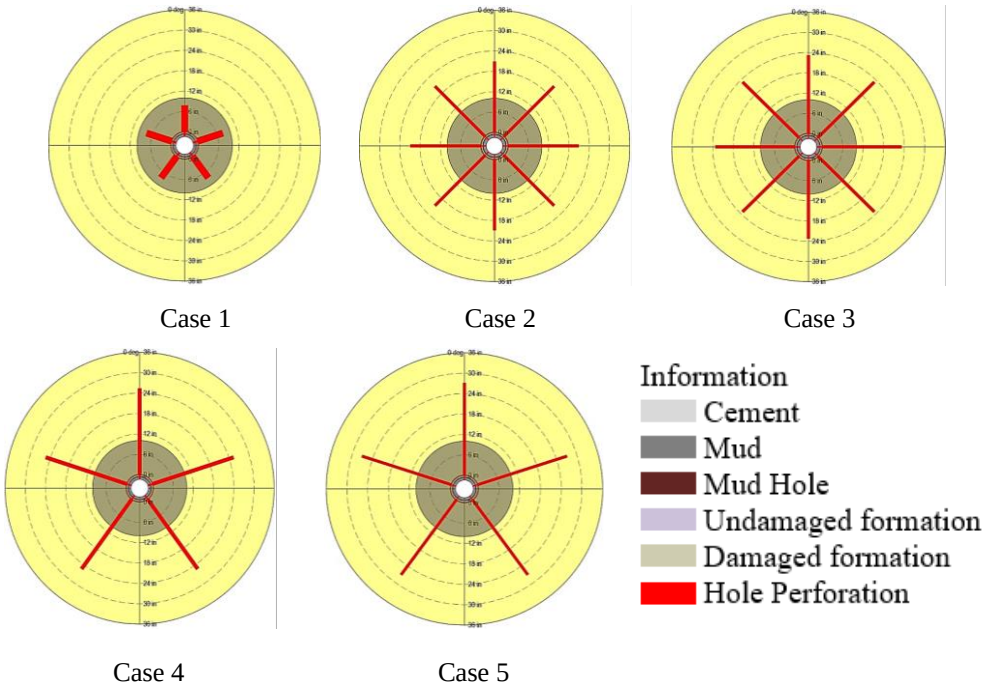

Figure 3. The Schematic Model of Perforation Geometry in Sandstone Layer 1 for Each Perforation System Case

3.2 Skin Effect Results of Perforation Geometry

Table 6 explains the results of the skin effect from various perforation systems used in the perforation modeling in each productive layer. The mechanical skin column represents the total sum of several skin components resulting from applied completions. Some of the skin criteria considered include the skin of the damage zone, perforation zone, and compacted zone.

Table 6. The Skin Effect Resulting from The Perforation System Modeling

Case	Perforation System	Mechanical skin				Damaged zone skin				Perforation & partial penetration skin				Compacted/crushed zone skin			
		Sandstone				Sandstone				Sandstone				Sandstone			
		1	2	3	4	1	2	3	4	1	2	3	4	1	2	3	4
1	*5" HSD 43C UltraPack RDX*	2,63	2,78	3,07	2,58	1,71	1,71	1,71	1,72	0,44	0,59	0,88	0,38	0,48	0,48	0,48	0,48
2	*4,72" PURE PowerJet Omega 3506 HMX*	-0,10	0,04	0,33	-0,16	-	-	-	-	-0,29	-0,15	0,14	-0,36	0,19	0,19	0,19	0,20
3	*4,72" PURE PowerJet Nova 3406 HMX*	-0,28	-0,13	0,16	-0,34	-	-	-	-	-0,44	-0,29	0,00	-0.50	0,16	0,16	0,16	0.16
4	*5" HSD, PowerJet Omega 4505 HMX*	0,19	0,33	0,62	0,13	-	-	-	-	-0,10	0,04	0,33	-0,17	0,29	0,29	0,29	0,30
5	*5" HSD PowerJet Nova 4505 HMX*	0,21	0,36	0,65	0,15	-	-	-	-	-0,12	0,03	0,32	-0,18	0,33	0,33	0,33	0,33

The damaged zone skin accounts for pressure losses when the reservoir fluid passes through a damaged zone in the formation. According to **Table 6**, the damaged zone skin component is only present in case 1 of the perforation system. In this case, perforation systems are unable to create holes that extend beyond the damaged zone. As a result, the fluid flow from the reservoir to the perforation hole experiences pressure losses within the damaged zone, leading to less efficient flow rates. On the other hand, perforation systems in cases 2 to 5 do not exhibit a damaged zone skin because they can create holes that surpass the damaged zone of the formation.

Perforation skin is a component that considers pressure losses when flow converges towards and through the perforation hole. It depends on the geometry of the perforation, including hole length, diameter, phase angle, and density. Partial penetration skin occurs when the productive layer is not fully completed or perforated, resulting in pressure losses. The ratio of perforation interval to productive layer *(Ip/I)* also affects partial penetration skin. For all productive layers, the *Ip/I* ratio is nearly 1, indicating minimal flow convergence due to partially completed productive layers. In **Table 6**, perforation systems in cases 2 to 5 exhibit very low values for perforation and partial penetration skin. This is because their perforation geometry, with longer hole lengths surpassing the formation-damaged zone, and an *Ip/I* ratio close to 1, reduce flow convergence towards the perforation hole.

Compacted/crushed zone skin is a skin component that forms due to the damage caused by the perforation process to the surrounding formation near the perforation hole. This damage reduces the permeability in the zone around the hole, resulting in pressure losses when fluid flows from the reservoir towards the perforation hole. The extent of compacted zone skin is influenced by the perforation geometry, particularly the length and diameter of the hole. **Table 6** shows that case 1 of the perforation system has the highest value of compacted zone skin compared to other cases. This is because this particular perforation system produces a sufficiently large perforation diameter, but the hole length is not enough to penetrate the formation damage. The use of high-explosive shaped charges in the perforation process causes the destruction of the formation, leading to the formation of compacted zone skin. The combination of a large perforation diameter and the presence of compacted zone skin in the formation damage zone worsens the pre-existing formation damage caused by fluid invasion, resulting in a higher skin value compared to other perforation systems.

After conducting an analysis and understanding the geometry and skin effects resulting from the modeling of various perforation systems, as explained above, the author has selected two cases: **case 1** representing conventional perforation, and **case 5** representing deep penetrating perforation. These two cases will be the focus of evaluation in this study.

3.3 High-energy Gas Fracturing Modeling Results

After inputting the data and performing several customizations of fluid properties, fracture dimensions, and pump scheduling, the modeled fracture geometry is obtained with the following details:

Table 7. The Data of Fracture Geometry Resulting from High-energy Gas Fracturing Modeling

Geometry Model	EOJ *Xf* (ft)	Propped *Xf* (ft)	EOJ height (ft)	EOJ Width (in)	Propped width (in)	Effective Conductivity (mD.ft)	Effective C_{FD}
P3D	46,4	48,9	74,5	1,403	0,912	1378	1,7

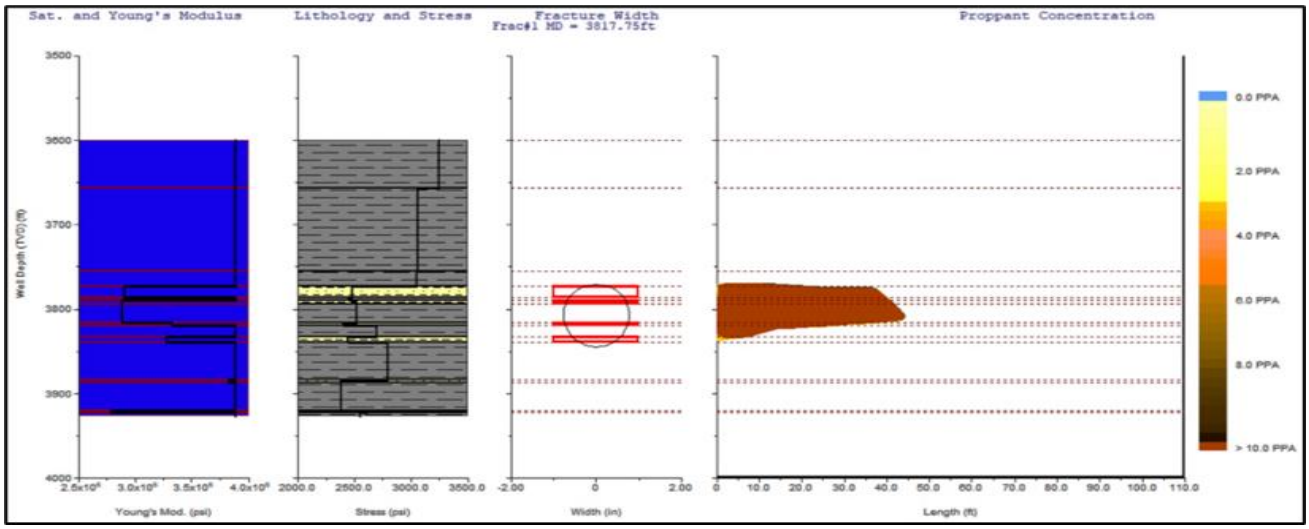

Figure 4. High-Energy Gas Fracturing Modeling Result: Fracture Geometry Scheme

This research utilizes a pseudo three-dimensional geometry (P3D) model for high-energy gas fracturing, which was selected based on the reservoir data conditions. The reservoir comprises multiple productive layers, with sandstone formations surrounded by shale layers. Fracture initiation within this model occurs at a depth of 3817.75 ft. The propagation of fractures in other productive layers is influenced by factors such as stress, thickness, and the proximity to the bounding shale layers (Economides et al., 1989).

Table 7 and **Figure 4** present the fracture geometry obtained from modeling high-energy gas fracturing using the hydraulic fracturing approach. The fracture length is 48.9 ft, with fracture height matching the interval of the existing perforations (74.5 ft), which accurately reflects real-life conditions in high-energy gas fracturing operations. The primary goal of high-energy gas fracturing is to eliminate the skin effect along the entire perforation interval. Notably, the end of job (EOJ) width, or the fracture width at the end of stimulation, measures 1.403 in. The author concludes that this fracture width can penetrate the perforation hole diameter in the formation (0.89 in), along with the thickness of the compacted zone (0.5 in), indicating the ability to fracture the compacted zone within each perforation interval. Consequently, the resulting fracture geometry is expected to improve the compacted zone around the perforation hole, leading to a negative skin effect.

In this study, the authors also identified the contour distribution of proppant concentration and fracture conductivity, as depicted in **Figure 5**. According to **Table 7**, the proppant coverage within the formed fracture measures 48.9 ft. The distribution of proppant concentration within the fracture exhibits variations, indicating that the concentration of proppant is not uniform from the fracture initiation point on the wellbore wall to the fracture tip. This inconsistency is attributed to the proppant carrying capacity of the fracturing fluid employed in the study. The utilized fracturing fluid was suboptimal in facilitating the transfer of proppant to the fracture tip, resulting in a diminishing proppant concentration towards the fracture tip. The suboptimal distribution of proppant concentration from the initiation point to the fracture tip also impacts the conductivity generated by the formed fracture.

Figure 5b illustrates that the fracture conductivity demonstrates favorable values in the segment near the wellbore wall (0 ft) up to 12.20 ft, with a fracture conductivity of 1481 mD-ft. As the proppant concentration decreases in subsequent segments towards the fracture tip, the fracture conductivity also diminishes, reaching a conductivity value of only 68 mD-ft. This phenomenon is attributed to both the suboptimal proppant carrying capacity of the fracturing fluid and the proppant factor used in the modeling. The customized proppant results in suboptimal permeability along the formed fracture. The segment close to the wellbore wall exhibits good conductivity, indicating favorable permeability in that region. Conversely, the segment approaching the fracture tip exhibits poor permeability, resulting in a lower conductivity value. The customized proppant's limited ability to withstand suboptimal closure pressure leads to reduced permeability as the fracture begins to close, particularly at the fracture tip.

The authors aimed to simulate real conditions in high-energy gas fracturing operations, where proppant injection is not performed. In this modeling, the customized proppant acts as fine rock grains or particles formed after the rock fracturing process, known as natural proppant, which provides new permeability and conductivity after fracturing. This result reflects the actual scenario in high-energy gas fracturing operations where proppant injection is not utilized (Zazozsky, 2004). The customized proppant in this modeling serves as fine rock grains or particles that form naturally after the rock fracturing process, contributing to the development of new permeability and conductivity following fracturing (Wenkui, et all., 2000).

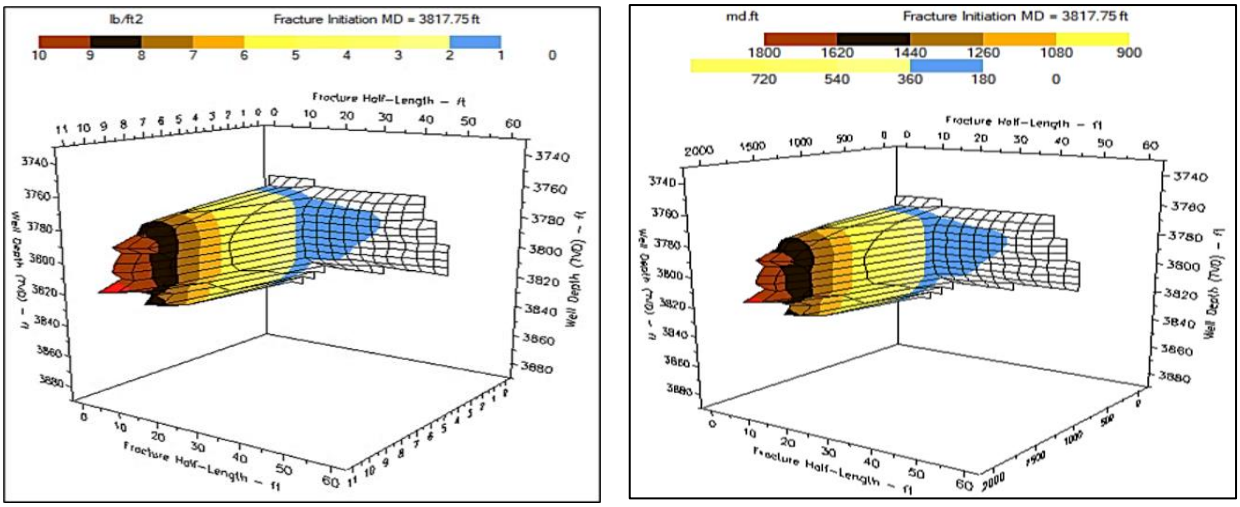

(a) (b)

Figure 5. (a) Proppant Concentration Contour, (b) Fracture Conductivity Contour

3.4 Productivity Evaluations

Author divides the productivity evaluations into three cases, which are: conventional perforation, deep penetrating perforation and combination of deep penetrating perforation and high-energy gas fracturing. The parameters that will be taken into accounts are: skin effect, PI and IPR.

a) Skin Effect Evaluation

Skin value from both perforation, conventional and deep penetrating operation, can be known directly from *Pipesim 2017* after conducting perforation modeling and it is already discussed at **Table 6. Table 8** below shows the resume of geometry and its skin value for both perforation systems.

Table 8. Geometry and Its Skin Value of Conventional and Deep Penetrating Perforation

Perforation System	Sandstones	Phase angle	Perforation density	Formation penetration avg. (in)	Formation diameter avg. (in)	Skin effect
5" HSD 43C UltraPack RDX (Conventional Perforation)	1	72	5	7,87	2,08	**2,63**
	2	72	5	7,87	2,08	**2,78**
	3	72	5	7,86	2,08	**3,07**
	4	72	5	7,85	2,08	**2,58**
5" HSD PowerJet Nova 4505 HMX (Deep Penetrating)	1	72	5	27,25	0,89	**0,21**
	2	72	5	27,24	0,89	**0,36**
	3	72	5	27,22	0,89	**0,65**
	4	72	5	27,21	0,89	**0,15**

For high-energy gas fracturing, the skin effect value must be estimated using Prats' method as discussed before. Data needed to estimate the skin value of high-energy gas fracturing are propped fracture half-length (*Xf*) and dimensionless fracture conductivity (C_{FD}) as seen in **Table 7.** Using Prats' graphic correlation (**Figure 2)**, C_{FD} of 1,7 is placed on axis 'x', then draw an apparent line vertically until intercept with the curve, and then draw an apparent line horizontally until intercept with the axis 'y', which is the ratio of effective well radius (r_w') over fracture half-length (*Xf*). Graphically the value of r_w'/Xf is 0,283, and multiplied by *Xf* (48,9 ft) to estimate the effective well radius (r_w') of 13,84 ft. From the value of r_w' (13,84 ft), skin effect after fracturing (*Sf*) can be estimated using **Equation 1**, and resulting a value of – 3,73.

b) Productivity Index (PI) Evaluation

The next step is PI evaluation for all cases using **Equation 2.** The data required and complete results of PI estimation for all cases can be seen in **Table 9.** As well as conventional and deep penetrating perforation, the case of combination of deep penetrating perforation and high-energy gas fracturing uses **Equation 2** to estimate the PI value. But in this case value of skin effect (*S*) is substituted to skin effect after fracturing (*Sf*) that has been estimated before (-3,73), resulting the PI value of 1,572.

Table 9. PI Evaluation for All Cases

Case	Sandstones	*k*, (mD)	*h*, (ft)	μ_o, (cP)	B_o, (RB/STB)	r_e, (ft)	r_w, (ft)	*S*	*PI*, (STB/d/psi)
5" HSD 43C UltraPack RDX (Conventional Perforation)	1	23	13,5	0,91706	1,185	220	0,333	**2,63**	**0,2217**
	2	23	4,5	0,91706	1,185	220	0,333	**2,78**	**0,0727**
	3	23	3,5	0,91706	1,185	220	0,333	**3,07**	**0,0548**
	4	23	7,5	0,91706	1,185	220	0,333	**2,58**	**0,1238**
5" HSD PowerJet Nova 4505 HMX (Deep Penetrating Perforation)	1	23	13,5	0,91706	1,185	220	0,333	**0,21**	**0,3016**
	2	23	4,5	0,91706	1,185	220	0,333	**0,36**	**0,0984**
	3	23	3,5	0,91706	1,185	220	0,333	**0,65**	**0,0734**
	4	23	7,5	0,91706	1,185	220	0,333	**0,15**	**0,1691**
Combination of Deep Penetrating Perforation and High-energy Gas Fracturing		23	29	0,91706	1,185	220	0,333	**-3,73**	**1,572**

c) Inflow Performance Relationship (IPR) Evaluation

Finally, the final evaluation of productivity result is IPR that can be estimated by constructing IPR curve using **Equation 3** and **Equation 4. Equations 4** are used for each well flowing pressure (*Pwf*) from 0 psi to equal to reservoir pressure (1200 psi). The complete value for constructing IPR for all cases can be seen in **Table 10** below.

Table 10. IPR Construction for All Cases

Pwf, (psia)	*IPR* Composite Conventional Perforation	*IPR* Composite Deep Penetrating Perforation	*IPR* Combination of Deep Penetrating Perforation and High-energy Gas Fracturing
	Q Oil, (STB/d)	Q Oil, (STB/d)	Q Oil, (STB/d)
0	315.44	428.41	1047,69
100	308.43	418.89	1024,41
200	297.91	404.61	989,49
300	283.89	385.57	942,92
400	266.37	361.77	884,72
500	245.34	333.21	814,87
600	220.81	299.88	733,38
690	195.73	265.83	650,09
700	192.77	261.80	640,26
800	161.22	218.96	535,49
900	126.17	171.36	419,08
1000	87.62	119.00	291,03
1100	45.56	61.88	151,33
1200	0.00	0.00	0,00

3.5 Productivity Comparison

The comparison of productivity results is carried out by comparing the values of skin, PI, and IPR. The values taken into consideration are the skin value and productivity index, which represent the well, while accounting for the four known productive sandstone layers.

a) Skin Effect and Productivity Index (PI) Comparison

The calculation of the skin value which represents the well is performed using the formula:

$$S_{avg} = \frac{Skin\ sandstone\ 1 + S\ sandstone\ 2 + S\ sandstone\ 3 + S\ sandstone\ 4}{4} \quad (5)$$

Meanwhile, the calculation of the Productivity Index (PI) is using the formula:

$$PI = \frac{k\,h}{141.2\,\mu_o\,B_o\left(\ln\frac{r_e}{r_w} + S_{avg}\right)} \quad (6)$$

Based on the formula, the values of the skin effect and PI are obtained as indicated in **Table 11**.

Table 11. Comparison of Skin and PI Results

Parameter	Conventional Perforation	Deep Penetrating Perforation	Combination of Deep Penetrating Perforation and High-energy Gas Fracturing
Skin effect	2,77	0,34	-3,73
PI, (STB/D/psi)	0,47	0,64	1,572

Based on the data presented in **Table 11** indicates that conventional perforation results in a significant skin value. This is due to the perforation system's inability to fully penetrate the damaged zone within the formation resulting in the presence of significant skin components such as damaged zone skin and compacted zone skin. The high skin value reflects severe formation damage, which in turn causes substantial pressure losses during fluid flow. Consequently, the reservoir's capacity to efficiently produce and deliver fluids to the wellbore is diminished, resulting in a low productivity index (PI).

In the case of deep penetrating perforation, a relatively low skin value is achieved. The skin components observed in deep penetrating perforation include perforation skin and compacted zone skin. The created perforation geometry surpasses the damaged zone within the formation, effectively eliminating the presence of damaged zone skin. The small skin value suggests that the formation damage caused by deep penetrating perforation is relatively minor. However, there are still pressure losses that hinder the optimal flow of production fluids to the wellbore, resulting in a comparatively lower productivity index (PI).

The negative skin value resulting from the combination of deep penetrating perforation and high-energy gas fracturing indicates the improvement of the formation. As previously explained, this formation improvement refers to the creation of fractures that can penetrate the damaged formation and enhance the conductivity of that zone. With increased conductivity, the reservoir's ability to flow fluids towards the wellbore is restored, resulting in a significant productivity index (PI) of 1.572 STB/D/psi.

Table 12 presents data on the productivity increase from three cases: conventional perforation, deep penetrating perforation, and the combination of deep penetrating perforation and high-energy gas fracturing. This data provides insights into the effectiveness of the combined technique in enhancing well production capability.

Table 12. PI Increments

Conventional Perforation	**Combination of Deep Penetrating Perforation and High-energy Gas Fracturing**	**Increment**
0,47 STB/D/psi	1,572 STB/D/psi	3,34 times
Deep Penetrating Perforation	**Combination of Deep Penetrating Perforation and High-energy Gas Fracturing**	**Increment**
0,64 STB/D/psi	1,572 STB/D/psi	2,45 times

Based on the obtained results, it is evident that the combination of deep penetrating perforation and high-energy gas fracturing yields a productivity increase of 2.45 times. In comparison with conventional perforation, it can achieve a productivity increase of up to 3.34 times. These findings align with the predicted range reported in previous studies by Dang Li et al. (1995) and Wenkui et al. (2000), where typical high-energy gas fracturing stimulation results in a productivity increase of 1.5 to 2.5 times compared to the pre-fracturing condition using the same perforation system. Thus, this research validates the effective optimization of reservoir potential in delivering fluids into the well by combining deep penetrating perforation and high-energy gas fracturing, resulting in improved well productivity compared to conventional perforation and deep penetrating perforation techniques.

b) Inflow Performance Relationship (IPR) Curve

Additionally, this study includes a comparison curve of the inflow performance relationship (IPR) for the three perforation cases, depicted in **Figure 6** below.

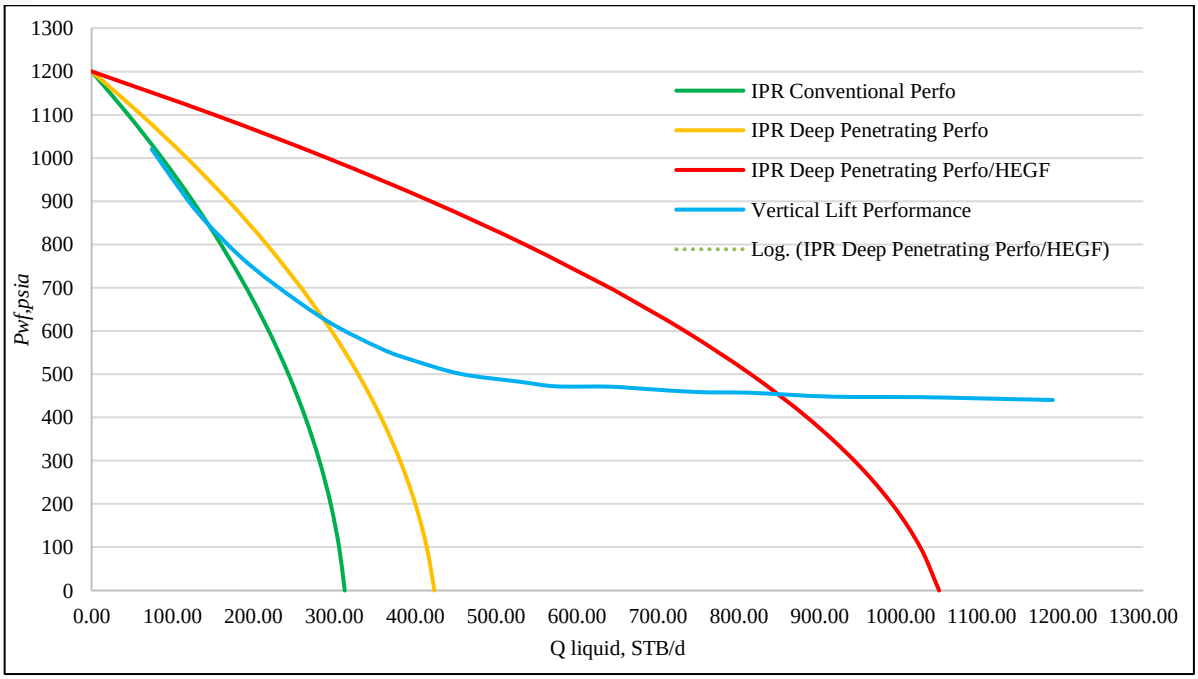

Figure 6. Comparison Results of IPR (Inflow Performance Relationship)

By analyzing the IPR graphic, it is evident that the combination of deep penetrating perforation and high-energy gas fracturing achieves the highest Absolute Open Flow Potential (AOFP) or maximum production rate. Furthermore, the intersection between the IPR curve and Vertical Lift Performance (VLP) allows us to determine the production rate through the tubing. The combination of deep penetrating perforation and high-energy gas fracturing yields a production rate of 850 STB/D, whereas deep penetrating perforation alone results in a production rate of 290 STB/D. In contrast, conventional perforation only generates a production rate of 150 STB/D.

In general, based on the comparison of skin effect, productivity index (PI), and inflow performance relationship (IPR), the combination of deep penetrating perforation and high-energy gas fracturing performs better than conventional perforation and deep penetrating perforation. This operational technique can achieve a negative skin effect, which significantly increases the productivity index (PI) and ultimately leads to a higher production rate. Therefore, it can be concluded that the combination of deep penetrating perforation and high-energy gas fracturing can effectively be applied to improve well productivity.

IV. CONCLUSION

Based on the conducted study, the following are the conclusions that can be drawn:

1. The combination of deep penetrating perforation and high-energy gas fracturing demonstrates the ability to generate perforation hole geometry that extends well beyond the formation-damaged zone. Additionally, it produces fractures with lengths reaching tens of feet (48.9 ft). These findings further validate the existing literature regarding the geometry achieved through the combined implementation of deep penetrating perforation and high-energy gas fracturing techniques.
2. The geometry resulting from the combination of deep penetrating perforation and high-energy gas fracturing effectively improves both the formation-damaged zone and compacted zone. This is supported by a negative skin value of -3.73 and a significant productivity index (PI) of 1.572 STB/d/psi.
3. The combination of deep penetrating perforation and high-energy gas fracturing can effectively enhance well productivity, resulting in a productivity increment of 3.34 times compared to conventional perforation and 2.45 times compared to deep penetrating perforation.

To further enhance this research, the author recommends developing a specialized simulator or software for modeling high-energy gas fracturing. Additionally, conducting an economic analysis on the combination of deep penetrating perforation and high-energy gas fracturing techniques is advised to determine their economic viability and success.

ACKNOWLEDGEMENTS

The authors would like to thank Prof. Dr. Ir. Sudjati Rachmat, DEA. (Alm. Abah) for guidance and support. Petroleum Engineering Department, Universitas Pembangunan Nasional "Veteran" Yogyakarta for the opportunity to publish this paper.

REFERENCES

Albert, L., Nery, N., Prapoo, H., Dai, P., Qu, B., Jiang, G., dan Kwok, D. (2018): Integrating propellant and shaped charges to improve frac efficiency – SPE-191785-MS, Society of Petroleum Engineers.

API Recommended Practice 19B (2001): Recommended practices for evaluation of well perforators – first edition, American Petroleum Institute, Washington D.C.

Economides, M. J., dan Nolte, K. G. (1989): Reservoir stimulation, Prentice Hall, Inc., New Jersey, 3-01 – 3-29.

El-Bermawy, H., dan El-Assal, H. (2001): A unique approach to enhancing production from depleted, highly laminated sand reservoirs using a combined propellant/perforating technique – SPE 68101, Society of Petroleum Engineers.

Feng, L., Mohammed, S., Ghaithan, A., dan Frank, F. C. (2015): Overview of existing proppant technologies and challenges – SPE-172763-MS, Society of Petroleum Engineers.

Guo, B., Lyons, W. C., dan Ghalambor, A. (2007): Petroleum production engineering, Elsevier Science & Technology Books, Oxford, 3/29 – 3/43.

Halleck, P. M. (1997): Recent advances in understanding perforator penetration and flow performance – SPE-27981-PA, Society of Petroleum Engineers.

Halliburton, (2017): Perforating solutions, Halliburton, 2.1 – 2.8.

Klotz, J. A., Krueger, R. F., dan Pye, D. S. (1974) Maximum well productivity in damaged formations requires deep, clean perforations – SPE 4792, Society of Petroleum Engineers.

Krueger, R. F. (1988): An overview of formation damage and well productivity in oilfield operations: an update – SPE-17459-MS, Society of Petroleum Engineers.

Lea, C. M., Hill, A. D., dan Sepehrnoorl, K. (1993): Effect of fluid diversion on the acid stimulation of a perforation – SPE-22853-PA, Society of Petroleum Engineers.

Liu, H., Wang, F., Zhang, J., Meng, S., dan Duan, Y. (2014): Fracturing with carbon dioxide application status and development trend - PETROL. EXPLORE. DEVELOP., 2014, 41(4): 513-519, Petroleum Exploration and Development.

Robert, J. W. (1982): Sandstone reservoir – SPE-10009-MS, Society of Petroleum Engineers.

Schechter, R. S. (1992): Oil well stimulation, Prentice Hall, Inc., New Jersey, 212 – 242.

Smith, M. B., dan Shlyapobersky, J. W. (2000): Basics of hydraulic fracturing, 5-1 – 5-28 dalam Economides, M. J., Boney, C. L., dan Dowell, S., Reservoir Stimulation in Petroleum Production.

Wenkui, L., dan Zhongtian, X. (2000): A review of gas fracturing technology – SPE-58980, Society of Petroleum Engineers.

Zazovsky, A. F. (2004): Propellant fracturing revisited – ARMA/NARMS 04-612, American Rock Mechanics Association.